1

In vitro/*in vivo* "peeling" of multilayered aminocarboxylate gold nanoparticles evidenced by a kinetically stable ^{99m}Tc-label: implications for glutathione-mediated drug release

Francisco Silva, Lurdes Gano, Maria Paula Cabral Campello, Rosa Marques, Isabel Prudêncio, Ajit Zambre, Anandhi Upendran, António Paulo* and Raghuraman Kannan*

The **BBN-Au-DTDTPA** coating is selectively released upon interaction with glutathione (GSH), rendering this nanoplatform potentially useful for GSH-mediated drug delivery.
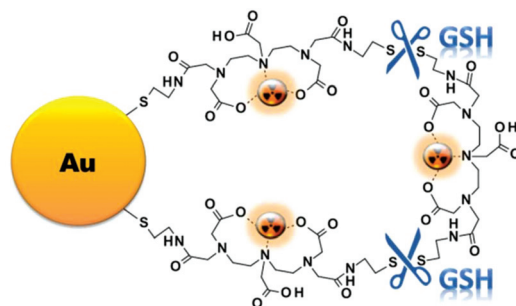
Q3

Please check this proof carefully. **Our staff will not read it in detail after you have returned it.**

Translation errors between word-processor files and typesetting systems can occur so the whole proof needs to be read. Please pay particular attention to: tabulated material; equations; numerical data; figures and graphics; and references. If you have not already indicated the corresponding author(s) please mark their name(s) with an asterisk. Please e-mail a list of corrections or the PDF with electronic notes attached – do not change the text within the PDF file or send a revised manuscript. Corrections at this stage should be minor and not involve extensive changes. All corrections must be sent at the same time.

Please bear in mind that minor layout improvements, e.g. in line breaking, table widths and graphic placement, are routinely applied to the final version.

We will publish articles on the web as soon as possible after receiving your corrections; **no late corrections will be made**.

Please return your **final** corrections, where possible within **48 hours** of receipt, by e-mail to: dalton@rsc.org

Queries for the attention of the authors

Journal: **Dalton Transactions**

Paper: **c7dt00864c**

Title: ***In vitro/in vivo* "peeling" of multilayered aminocarboxylate gold nanoparticles evidenced by a kinetically stable ^{99m}Tc-label: implications for glutathione-mediated drug release**

Editor's queries are marked like this [Q1 , Q2 , ...], and for your convenience line numbers are indicated like this [5, 10, 15, ...].

Please ensure that all queries are answered when returning your proof corrections so that publication of your article is not delayed.

Query Reference	Query	Remarks
Q1	For your information: You can cite this article before you receive notification of the page numbers by using the following format: (authors), Dalton Trans., (year), DOI: 10.1039/ c7dt00864c.	
Q2	Please carefully check the spelling of all author names. This is important for the correct indexing and future citation of your article. No late corrections can be made.	
Q3	Please check that the Graphical Abstract text fits within the allocated space indicated on the front page of the proof. If the entry does not fit between the two horizontal lines, then please trim the text and/or the title.	
Q4	The sentence beginning "Transmission electron microscope images..." has been altered for clarity, please check that the meaning is correct.	
Q5	The author's name is spelled "Prudencio" in ref. 37 and 38, but in the text it is spelled "Prudêncio". Please check and correct as necessary.	
Q6	The sentence beginning "Such kinetic inertness supports..." has been altered for clarity, please check that the meaning is correct.	
Q7	The sentence beginning "Second, the GSH-mediated release..." has been altered for clarity, please check that the meaning is correct.	
Q8	Ref. 8 and 44: Please provide the page (or article) number(s).	
Q9	Ref. 21: Please provide details of the last page number for this article.	

Q1

Q2

In vitro/in vivo "peeling" of multilayered aminocarboxylate gold nanoparticles evidenced by a kinetically stable ^{99m}Tc-label: implications for glutathione-mediated drug release†

Francisco Silva,[a] Lurdes Gano,[a] Maria Paula Cabral Campello,[a] Rosa Marques, [a] Isabel Prudêncio,[a] Ajit Zambre,[b] Anandhi Upendran,[c] António Paulo *[a] and Raghuraman Kannan*[b,d]

A thiolated bombesin peptide was conjugated to **Au-DTDTPA** nanoconstructs to obtain **BBN-Au-DTDTPA** targeted to the gastrin releasing peptide receptor (GRPr). Different analytical techniques showed that this conjugate shares similar physico-chemical properties with **Au-DTDTPA**; HPLC and XPS analyses corroborated the attachment of the bioactive peptide to the AuNPs surface. Competitive binding assays in PC3 cancer cells showed that these BBN-containing AuNPs have high affinity for GRPr. **BBN-Au-DTDTPA** was successfully radiolabeled with ^{99m}Tc and showed high in vitro stability towards different biological media and substrates, except for glutathione (GSH). In vitro and in vivo studies, based on gamma-counting (^{99m}Tc content) and nuclear activation analysis (Au content), indicated the release of the DTDTPA coating from the AuNPs. Probably, the "peeling" of the layered-aminocarboxylate coating is GSH-mediated and involves the cleavage of the DTDTPA disulfide bonds and/or Au–S bonds. These results render **BBN-Au-DTDTPA** an interesting platform deserving further evaluation in target-specific GSH-mediated drug delivery.

Introduction

The recent years have seen a wide variety of reports on the potential applications of nanoparticles in the field of cancer theranostics.[1–4] This reflects the favourable physico-chemical features of the nanoconstructs for biomedical use, such as their optical, electronic, and magnetic properties, as well as the possibility of their conjugation to a plethora of different medically relevant chemical entities, ranging from peptides, antibodies, proteins, and chemotherapeutic drugs to metal chelators.[5–10] Among their variety of applications, the use of nanoparticles as drug delivery platforms to tumor sites is another topic of great interest among researchers. The two important factors that guide drug delivery are: (1) conjugation

of therapeutic molecules to the nanocarrier (either by physical adsorption, covalent attachment or encapsulation); (2) release of the therapeutic payload from the nanocarrier to perform its function.

Triggered-release drug delivery tools based on nanoparticle platforms have been previously studied, in which the payload release can be done through a variety of stimulations, such as photo- or thermal-exposure, enzymatic reaction, or low level pH in tumor tissues. Another approach that has attracted much attention in this regard is glutathione (GSH)-mediated release.[11–15] GSH is capable of cleaving disulfide bonds through a reductive reaction and in vivo, it is in a significantly high concentration intracellularly (1–10 mM), while in the extracellular environment it is present in a low amount (2 μM). Developing new nanoparticle tools for GSH-mediated drug release can be challenging, as in most cases it is difficult to assess the biological fate of the nanoconstruct in vivo and that of the released molecule after GSH cleavage. There are several studies reported in the literature about GSH-mediated drug delivery from AuNP systems, profiting from the aurophilicity of GSH.[16–18]

Radiolabeled nanoparticles can give important insights to address the above-mentioned issues, as the presence of the radioactive label allows a non-invasive and quantitative follow-up of the biological fate of the nanoparticles and/or respective

[a]Centro de Ciências e Tecnologias Nucleares, Instituto Superior Técnico, Universidade de Lisboa, Estrada Nacional 10, Km 139.7, 2695-066 Bobadela LRS, Portugal. E-mail: apaulo@ctn.tecnico.ulisboa.pt
[b]Department of Radiology, University of Missouri-Columbia, Columbia, Missouri-65212, USA
[c]Institute of Clinical and Translational Science, School of Medicine, University of Missouri-Columbia, Columbia, Missouri-65212, USA
[d]Department of BioEngineering, University of Missouri-Columbia, Columbia, Missouri-65212, USA. E-mail: kannanr@health.missouri.edu
†Electronic supplementary information (ESI) available. See DOI: 10.1039/c7dt00864c

coating and payload, depending on how and which radiolabel is introduced in the nanoconstruct. Several medically relevant radionuclides can be utilized for the labeling of nanoparticles. Most importantly, many of them correspond to radioisotopes that have already been incorporated in clinically approved radiopharmaceuticals for diagnostic nuclear medicine by single photon emission computed tomography (SPECT) (*e.g.* [99m]Tc, ^{67}Ga, ^{111}In) or positron emission tomography (PET) (*e.g.* [18]F, ^{68}Ga, ^{64}Cu).[19] In general, it is important to ensure that the "reporter" radionuclide always travels inside the body together with the labeled nanocarrier to have a true and reliable picture of its biodistribution. The introduction of appropriate radiolabels at the core or on the surface coated ligands of the nanoparticles can be helpful to study *in vivo* the structural integrity of the nanoconstruct, and obtain confirmation of coating or payload release from the nanoparticle structure.[4,20] A representative example of this approach has been recently reported by Kreyling *et al.*, who have proved the *in vivo* release of an organic polymer coating conjugated to gold nanoparticles (AuNPs) by studying the biodistribution of the nanoconstructs based on its [198]Au-labeled gold core and its ^{111}In-labeled polymeric coating.[21]

Gold nanoparticles can be easily functionalized with target-specific biomolecules and chelators for a stable complexation of radiometals. The most common strategies for the functionalization of AuNPs involve the formation of gold–thiol covalent bonds between gold atoms from the surface of the nanoparticle and thiol groups from the grafted molecule.[22,23] These strategies have been already successfully applied in a few instances to achieve a target-specific delivery of radiometals to tumor tissues, namely, strategies based on AuNPs conjugated with bombesin (BBN) peptide analogs recognizing the gastrin releasing peptide receptor (GRPr) that is overexpressed in a series of human cancers.[10,24–28] We have recently described a novel BBN-containing nanoconstruct, stabilized by a new macrocyclic DOTA derivative (trimethyl 2,2′,2″-(10-2(3-(tritylthio)propamido)ethyl)-1,4,7,10-tetraazacyclododecane-1,4,7-trityl)triacetate (TDOTA) that allowed also a stable coordination of [67]Ga[3+] in biological milieu. The resulting radiolabeled nanoconjugates displayed a remarkably high cellular internalization in human prostate cancer PC3 cells that are known to overexpress the GRPr.[26]

Our team has also worked with congener AuNPs with similar core sizes (3–5 nm) coated with a thiolated DTPA derivative (2-[bis[2-[carboxymethyl-[2-oxo-2-(2-sulfanylethylamino)ethyl]amino]ethyl]amino]acetic acid (**DTDTPA**)). However, these AuNPs were unable to coordinate [67]Ga[3+] in a kinetically stable way and the coordinated [67]Ga[3+] undergoes fast transchelation processes in the presence of *apo*-transferrin or cell medium.[26,29] These **Au-DTDTPA** nanoplatforms were introduced originally by Roux *et al.* who have evaluated their usefulness as X-ray contrast agents or as radiosensitizers.[30,31] The same authors have also demonstrated that these **Au-DTDTPA** can coordinate to gadolinium, showing very promising results as contrast agents for MRI imaging.[32] Furthermore, the same team also showed that **Au-DTDTPA** can be directly labeled with ^{99m}Tc and ^{111}In by reaction with [99m]TcO$_4^-$/Sn^{2+} and [111]InCl$_3$, respectively.[33]

The DTDTPA coating is polymerized around the nanoparticle structure through disulfide bonds, and we have hypothesized that these S–S bonds or the Au–S bonds could be selectively cleaved by GSH. If this should be the case, **Au-DTDTPA** would have potential relevance as target-specific GSH-mediated drug releasing tools. Previously we have shown that the DTDTPA coating can be functionalized with biomolecules such as the horseradish peroxidase (HRP), a model molecule that was conjugated to the carboxylic groups of DTDTPA.[34] The same type of strategy can be readily explored for the conjugation of a cytotoxic drug that can be eventually released from the AuNP surface by GSH-mediated cleavage of S–S or Au–S bonds.

As a proof of concept for GSH-mediated drug release, we functionalized **Au-DTDTPA** nanoparticles with a thiolated derivative of BBN, a peptide with well-recognized biological specificity towards prostate cancer cells that overexpress the GRPr.[26] Furthermore, we have studied the ^{99m}Tc-labeling of the resulting BBN-containing nanoconjugates using the so-called tricarbonyl approach. We hypothesized that DTDTPA would provide a stable complexation of the *fac*-[[99m]Tc(CO)$_3$]$^+$ core, in contrast to the results that we have previously reported for [67]Ga[3+].[26] Unlike [67]Ga[3+], [[99m]Tc(CO)$_3$]$^+$ should be kinetically stable to allow the follow-up of the *in vitro*/*in vivo* fate of the DTDTPA coating.

In this work, we report the functionalization of **Au-DTDTPA** nanoparticles with a BBN peptide analog, their physicochemical characterization by a variety of techniques, including UV-Vis, transmission electron microscopy (TEM), dynamic light scattering (DLS) and X-ray photoelectron spectroscopy (XPS) measurements, as well as their binding affinity towards the GRPr that was assessed by competitive binding assays using PC3 cells. A study of the radiolabeling of these nano-bioconjugates with the *fac*-[[99m]Tc(CO)$_3$]$^+$ core is also presented, together with the evaluation of their *in vitro* stability in the presence of different media, including GSH, and *in vivo* stability and biodistribution in normal mice. Altogether, these studies were expected to provide an insight on the possible GSH-mediated release of DTDTPA from the nanoparticles in an *in vivo* environment and, therefore, on the potential relevance of these AuNPs for controlled drug release.

Methods

General procedures

The materials used for synthesis of the AuNPs were procured from standard vendors. All reagents and solvents were commercially acquired from Aldrich. Na[[99m]TcO$_4$] was eluted from a commercial [99]Mo/^{99m}Tc generator, using a 0.9% saline solution. [[99m]Tc(H$_2$O)$_3$(CO)$_3$]$^+$ was prepared by labeling of a Isonlink®-kit with Na[[99m]TcO$_4$], following a procedure described elsewhere.[35] For the preparation of aqueous solutions and for rinsing of gold nanoparticles, Milli-Q (DI) water

was used. DTDTPA and **Au-DTDTPA** were synthesized according to previously published methods.[30,34]

UV-visible spectroscopy. UV-visible absorption spectra were recorded at room temperature using a Varian Cary 50 UV-Vis spectrophotometer in disposable or quartz cuvettes with a 10 mm path length.

Transmission electron microscopy (TEM). Transmission electron microscope images were obtained on a JEOL 1400 TEM, JEOL Ltd, Tokyo, Japan. TEM samples were prepared by placing 5 μL of gold nanoparticle solution on the 300 mesh carbon coated copper grid, and the solution was allowed to remain for five minutes. Excess solution was removed carefully and the grid was allowed to dry for an additional five minutes. The average size and size distribution of the nanoparticles were determined by processing the TEM image Adobe Photoshop with Fovea plug-ins.

Dynamic light scattering (DLS). DLS measurements were performed with a Malvern Zetasizer Nano ZS (Malvern Instruments Ltd, USA) equipped with a 633 nm He–Ne laser and operating at an angle of 173°. The software used to collect and analyze the data was the Dispersion Technology Software (DTS) version 5.10 from Malvern. 600 μl of each sample was measured in low volume semi-micro disposable sizing cuvettes (Fisher Scientific, USA) with a path length of 10 mm. Triplicate measurements were made at a position of 4.65 mm from the cuvette wall with an automatic attenuator. For each sample, 15 runs of 10 seconds were performed. The size distribution, the Z-average diameter (Z-ave) and the polydispersity index (PDI) were obtained from the autocorrelation function using the "general purpose mode" for all nanoparticle samples. A default filter factor of 50%, default lower threshold of 0.05 and upper threshold of 0.01 were used. Zeta potential measurements were performed in triplicate using water as the dispersant and the Huckel model was followed. For each sample, 20 runs were performed in auto analysis mode.

X-ray photoelectron spectroscopy (XPS). XPS analysis was performed by Rocky Mountain Labs Inc., Colorado, USA, in a Kratos XSAM800 spectrometer, operated in the fixed analyser transmission (FAT) mode, with a pass energy of 20 eV and a power of 120 W and using non monochromatic Al Kα and Mg Kα radiations.

High performance liquid chromatography (HPLC). HPLC analyses were performed in a PerkinElmer LC200 pump with a UV-visible Shimadzu LC290 and a Berthold LB-507A γ-detector, using a Macherey-Nagel EC 250/4 Nucleaosil 100-5 C18 with a flow rate of 0.5 mL min^{-1}. The solvents used were HPLC grade; H_2O was bidistilled and filtered in 0.22 μm Millipore filters. Solvents: A = TFA 0.1% (aq.), B = MeOH. Gradient: 10 min (100% A), 10 min (100% B), 20 min (100% B), 1 min (100% A), 9 min (100% A).

Synthesis of TA-BBN. Thiotic acid terminated bombesin peptide was prepared as reported previously,[27,28] in an automated peptide synthesizer (Liberty; CEM, Matthews, NC, USA). Following the coupling of all the amino acids in the appropriate sequence, thiotic acid was coupled using a mixture of DIC/HOBt. Cleavage from the resin and removal of the amino

acid side chain protecting groups of the peptides were performed using a solution of TFA/thioanisole/H_2O (95 : 2.5 : 2.5), and finally, purification by HPLC was done.

Synthesis of BBN-Au-DTDTPA. Thiotic acid terminated bombesin was reacted with DTDTPA stabilized gold nanoparticles with stoichiometric ratios of Au : BBN 1 : 0.25, 1 : 0.5, 1 : 1, 1 : 2 and 1 : 4. Typically, in a 20 ml glass vial, a solution of **Au-DTDTPA** ([Au] = 2.28 μmol) using aqueous/methanolic mixture (1 : 9) of 0.01 M NaOH was prepared. Thiotic acid terminated bombesin (**TA-BBN**) 0.64 mg (0.57 μmol), 1.28 mg (1.14 μmol), 2.56 mg (2.27 μmol), 5.12 mg (4.54 μmol) and 10.24 mg (9.08 μmol) were dissolved in 4 mL of MeOH and then added to the nanoparticle solution. The reaction mixture was stirred for 2 hours at room temperature and formation of a dark brown precipitate was observed. The mixture was centrifuged (12 000 rpm for 5 min at 20 °C) and the supernatant was removed. The precipitated AuNPs were washed two times with MeOH and three times with water. The washed AuNPs were dried at low pressure and stored at −20 °C.

IC$_{50}$ measurements. The receptor binding affinities of the BBN conjugated gold nanoconstructs were determined by a competitive cell-binding assay on PC-3 cell cultures using ^{125}I-Tyr4-bombesin as the GRP specific radio-ligand. Approximately 30 000 cells were incubated at 37 °C for 40 minutes under 5% CO_2 in the presence of 20 000 cpm ^{125}I-Tyr4-bombesin (2200 Ci mmol^{-1}) and an increasing concentration of the gold nanoconjugates. After incubation, the reaction medium was aspirated, and the cells were washed three times with cold RPMI 1640 modified buffer. Cell-associated radioactivity was determined by counting in a Packard Riastar γ counting system. IC$_{50}$ values were calculated using GraphFit 4.0 graphing software.

Radiolabeling BBN-Au-DTDTPA with ^{99m}Tc. 25 μL of a solution of **BBN-Au-DTDTPA** (5 mg mL^{-1}, H_2O) were placed in a 10 mL glass vial. The vial was encapsulated and purged with N_2. 500 μL of $[^{99m}Tc(H_2O)_3(CO)_3]^+$, previously adjusted to pH ≈ 7, was added. The mixture was heated at 100 °C for 30 min. The solution was centrifuged (12 000 rpm for 5 min at 20 °C) and the supernatant was removed. The precipitated AuNPs were washed three times with water. Purity control was performed by TLC using MeOH/HCl (6 M) 95 : 5 as eluent in ITLC-SG.

Radiolabeling DTDTPA with ^{99m}Tc. 50 μL of a solution of DTDTPA (0.02 M, H_2O) were placed in a 10 mL glass vial. The vial was encapsulated and purged with N_2. 500 μL of $[^{99m}Tc(H_2O)_3(CO)_3]^+$, previously adjusted to pH ≈ 7, was added. The mixture was heated at 100 °C for 30 min. Radiochemical yield was performed by HPLC (>99%) and the radioactive compound was used without further purification.

Radiolabeling GSH with ^{99m}Tc. 20 μL of a solution of GSH (0.02 M, H_2O) were placed in a 10 mL glass vial. The vial was encapsulated and purged with N_2. 180 μL of $[^{99m}Tc(H_2O)_3(CO)_3]^+$, previously adjusted to pH ≈ 7, was added. The mixture was heated at 100 °C for 30 min. Radiochemical yield was performed by HPLC.

Stability studies. Stability studies for **BBN-Au-DTDTPA-^{99m}Tc** were performed by incubation in the presence of different

media: 0.1 M PBS, 0.9% NaCl, cell culture medium, histidine (0.02 M) and glutathione (0.02 M). To 30 μL of the ^{67}Ga-labelled AuNPs were added 120 μL of the different challenging solutions, and the resulting mixtures were incubated at 37 °C for different intervals of time (0–24 h). For each time point, the radiochemical purity of the **BBN-Au-DTDTPA-[99m]Tc** was assessed by TLC using MeOH/HCl (6 M) 95 : 5 as eluent in ITLC-SG.

Biodistribution studies. Animal studies were conducted in conformity with the national law and with the EU Guidelines for Animal Care and Ethics in Animal Experimentation. The animals were housed in a temperature- and humidity-controlled room with a 12 h light/12 h dark schedule. Biodistribution of the radioactive compounds was evaluated in CD-1 mice. The animals were intravenously (i.v.) injected by tail vein administration of the compounds (1.5–6.0 MBq) diluted in 100 μL of NaCl 0.9%. The dose administered and the radioactivity in the sacrificed animals were measured using a dose calibrator (Capintec CRC25R). The difference between the radioactivity in the injected and sacrificed animals was assumed to be due to excretion. The tissues of interest were dissected, rinsed to remove excess blood and weighed, and their radioactivity was measured using a γ-counter (LB2111, Berthold, Germany). The uptake of radioactive compounds in the tissues was calculated and expressed as a percentage of the injected radioactivity dose per gram of tissue. To measure the Au content, blood, liver and pancreas were frozen immediately after radioactivity measurement and allowed to decay before sample treatment for nuclear activation analysis. Urine was also collected and pooled together at the time the animals were sacrificed. TLC control of the urine was performed using MeOH/6 M HCl (95 : 5) as eluent in ITLC-SG. The urine samples were centrifuged at 5000 rpm for 5 min before injection in the HPLC.

Nuclear activation analysis (NAA). Primary standard solutions containing gold were prepared and dispersed onto cellulose in cleaned high-density polyethylene vials, and used as standards. Prior to analysis, the blood tissues, liver and pancreas were freeze-dried and ground in a Teflon™ mill. Then the samples were weighted into identical polyethylene vials. A similar geometry was used for both standards and samples.

The three standards and all the samples were irradiated together for 4 h in the core grid of the Portuguese Research Reactor (CTN/IST, Bobadela) at a thermal flux of 3.96×10^{12} n cm^{-2} s^{-1}; $\phi_{th}/\phi_{epi} = 96.8$; $\phi_{th}/\phi_{fast} = 29.8$.[36] The bundles were rotated continuously during irradiation to ensure that all the samples received the same exposure to neutrons. Even so, Fe flux monitors were placed in appropriate plastic containers for irradiation together with the samples and standards for neutron flux variation corrections. Gamma-ray spectrometry was carried out after a delay of 7 to 9 days. A high purity germanium detector with nominal resolutions (FWHM) of 450 eV at 5.9 keV and 2100 eV at 122 keV was used to quantify the 412 keV peak from [198]Au. Details of the analytical method may be found elsewhere (Gouveia *et al.*, 1992, Gouveia and Prudêncio, 2000).[37,38]

Results

Functionalization with the bioactive peptide: synthesis of BBN-Au-DTDTPA

The **Au-DTDTPA** nanoconjugate was obtained based on the method reported by Roux *et al.* by reduction of HAuCl$_4$·3H$_2$O with NaBH$_4$ in the presence of excess DTDTPA.[30] As previously described, in these nanoparticles DTDTPA forms a multi-layered coating around the gold core as a result of a catenation process due to the formation of S–S bonds between independent units of DTDTPA.[30] Therefore, the surface bound DTDTPA is rich in disulfides, secondary amines and carboxylates. Previously the free carboxylate groups from **Au-DTDTPA** were explored for conjugation with biomolecules, namely the enzyme horseradish peroxidase (HRP).[34] Alternatively, in this work we have sought to explore the possibility of attaching BBN analogs to **Au-DTDTPA** based on the formation of Au–S bonds. For this purpose, we focused on a BBN analog (**TA-BBN**) that contains the eight aminoacid BBN [7–14] sequence and a thioctic acid group (**TA**) for conjugation to the surface of the AuNPs[26–28]

The functionalization of **Au-DTDTPA** with **TA-BBN** was performed by reacting the **AuNPs** with the peptide in methanol at room temperature using different **Au : TA-BBN** molar ratios (1 : 0.24, 1 : 0.4, 1 : 0.8, 1 : 2 and 1 : 4) (Scheme 1). After 2 h of reaction, the resulting functionalized nanoconstruct (**BBN-Au-DTDTPA**) was separated from the supernatant by filtration, followed by washing with MeOH to remove any non-reacted **TA-BBN**, and finally washed with H$_2$O.

The amount of **TA-BBN** conjugated to **Au-DTDTPA** was determined based on the HPLC analysis of the supernatants of the different reaction mixtures and comparison with the starting **TA-BBN** solutions (Fig. 1). The differences in the **TA-BBN** peak areas, before and after reaction, were used to quantify the amount of peptide conjugated to the AuNPs. The maximum amount of **TA-BBN** that can be conjugated to **Au-DTDTPA** is ≈0.26 mg mg^{-1} of nanoparticles. Saturation of the AuNP surface with the peptide was achieved when the conjugation of the peptide is performed using a molar ratio of at least 1 : 2 (**Au : TA-BBN**). As previously reported by our group,[34] nanoparticle tracking analysis (NTA) of **Au-DTDTPA** indicated that there are 1.67×10^{14} nanoparticles per mg of compound; based on this value it was possible to estimate the number of **TA-BBN** molecules conjugated to each AuNP, which is roughly 53 units of **TA-BBN** at the saturated nanoparticle surface.

Binding affinity and physico-chemical characterization of BBN-Au-DTDTPA

We investigated the *in vitro* binding affinity of BBN upon conjugation to AuNPs and the influence of peptide payload on GRPr-affinity. Competitive binding assay experiments were performed with the commercially available radiopeptide ^{125}I-Tyr$_4$-BBN using prostate cancer PC3 cells that are known to overexpress GRPr. The binding affinity towards PC3 cells was evaluated for all three nanoconstructs prepared with different molar ratios (Au : **TA-BBN** molar ratio of 1 : 0.4, 1 : 2 and 1 : 4).
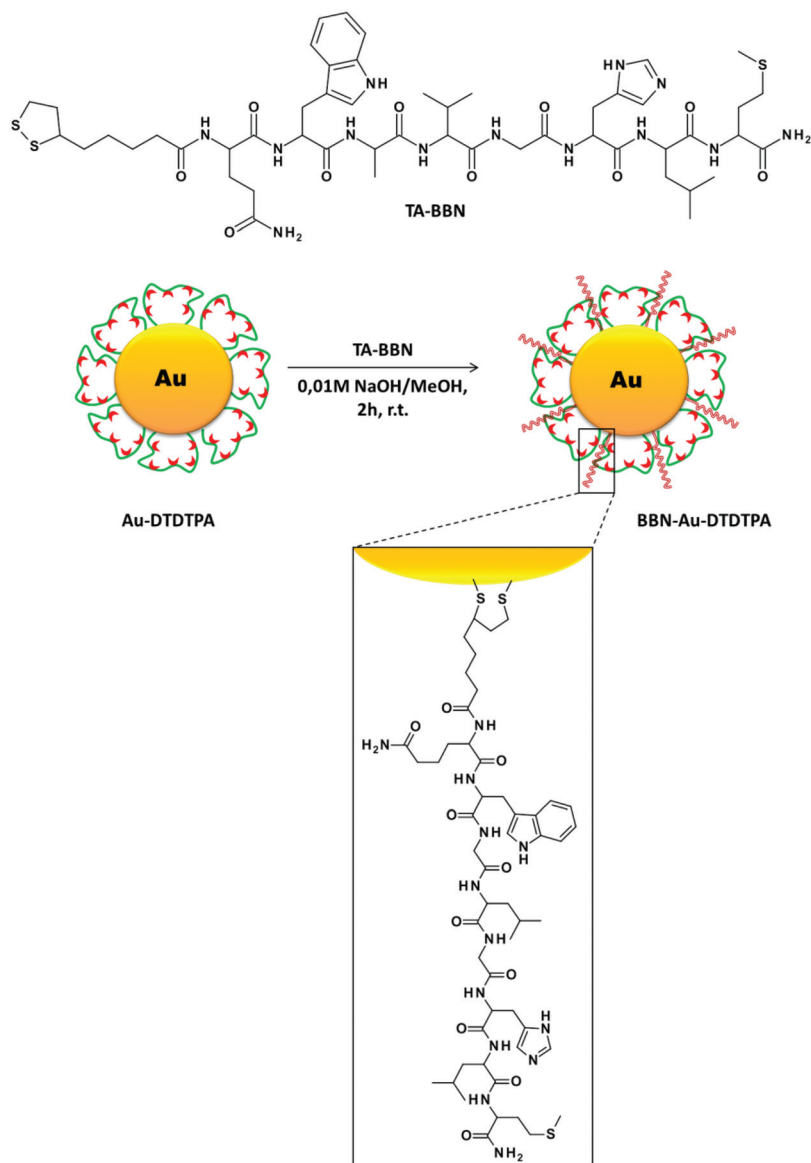
Scheme 1 Structure of **TA-BBN** and synthesis of **BBN-Au-DTDTPA**.

The binding affinities of the nanoconstructs varied with the amount of conjugated **TA-BBN**, and the measured IC_{50} values ranged between 0.6 and 0.02 μg mL^{-1}, as depicted in Fig. 2. This trend indicates that the **TA-BBN** peptides attached to the nanoparticle surface still recognize the GRPr in a concentration-dependent manner. In particular, the **BBN-Au-DTDTPA** nanoparticles obtained with a molar ratio of 1 : 2 (Au : **TA-BBN**) display a binding affinity (IC_{50} = 0.1 μg mL^{-1}) comparable to that exhibited by **Au-TDOTA** (IC_{50} = 0.045 μg mL^{-1}) functionalized with the same BBN derivative.[26] These **BBN-Au-DTDTPA** nanoconjugates are saturated with **TA-BBN**, and were used for further physico-chemical characterization and ^{99m}Tc-labelling studies.

BBN-Au-DTDTPA was characterized by UV-Vis spectroscopy, TEM analysis, DLS and zeta-potential measurements (Fig. 3), aiming to assess the influence of the incorporation of the BBN peptide in the physico-chemical properties of the AuNPs.

As shown in Fig. 3, the UV-Vis spectrum of **BBN-Au-DTDTPA** shows a broad absorption band centered at ≈520 nm, similar to **Au-DTDTPA**. This indicates that the conjugation of **TA-BBN** to the AuNPs did not alter the core size of the nanoparticles, and was corroborated by the TEM analysis of **BBN-Au-DTDTPA** (≈2 nm; Fig. 3c).

By contrast, the hydrodynamic size of **BBN-Au-DTDTPA** in water (≈146.2 nm) is slightly higher than that of **Au-DTDTPA** (≈100.6 nm), in agreement with an increasing radius of the AuNP coating due to the conjugation of **TA-BBN** (Fig. 3b). On the other hand, there is minimal change in the zeta-potential values of **BBN-Au-DTDTPA** (−71.5 ± 9.1 mV) compared with that of **Au-DTDTPA** (−80.7 ± 15.6 mV), showing that the pres-
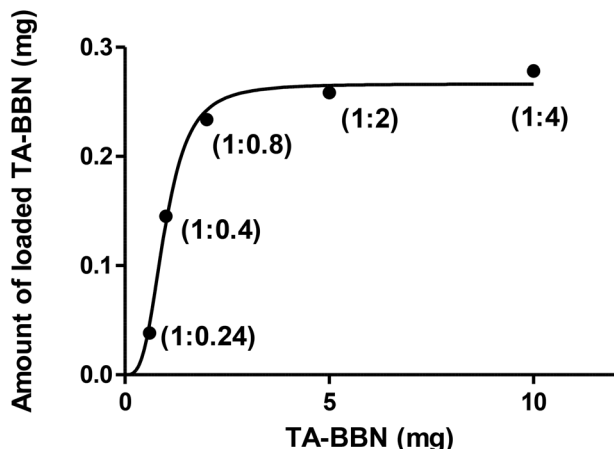
Fig. 1 Amounts of **TA-BBN** loaded into 1 mg of **Au-DTDTPA** as a function of the Au : TA-BBN molar ratio.
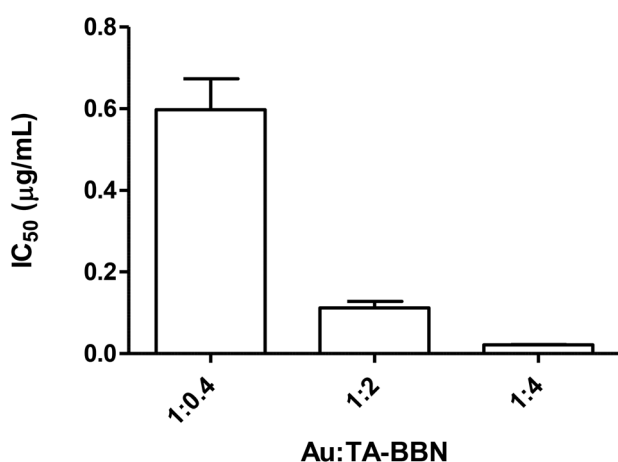
Fig. 2 IC$_{50}$ values measured for **BBN-Au-DTDTPA** synthesized using different Au : TA-BBN molar ratios. Measurements were done in prostate cancer PC3 cells by competition binding experiments with the radio-peptide ^{125}I-Tyr$_4$-BBN.

ence of **TA-BBN** did not affect much the highly negative charge character of the nanoconstruct and indicating the high stability of the particles.[34]

BBN-Au-DTDTPA was also characterized by XPS (see Fig. S1†). The obtained high-resolution XPS spectra revealed the presence of S 2p$_{3/2}$ and S 2p$_{1/2}$ energy bands, ranging between 162.3 eV and 164.4 eV. These bands are most likely due to the presence of covalent Au–S bonds, and disulfide bonds of the **DTDTPA** coating and thioether bonds from the methionine group of the BBN derivative.[39] The high resolution XPS spectrum of the C 1s region indicates two distinct binding energy bands, centered at ≈285 eV and ≈288 eV. The deconvolution of the first band gives rise to two types of C 1s bindings, one with binding energy at ≈285 eV (C–C and C–H from methylenic groups) and another one showing slightly higher binding energy levels at ≈286 eV (C–N groups).[39] The second C 1s band, centered at ≈288 eV, corresponds to the C–O binding

energies of COOH and CONH.[39] The intensity of this band is much higher than in the XPS spectrum of **Au-DTDTPA**. This is most likely due to the presence of the peptide which has a high amount of amino acid groups, therefore corroborating the attachment of the BBN derivative to the AuNPs surface.

Radiolabeling with fac-[^{99m}Tc(CO)$_3$]$^+$ and in $vitro$ stability studies

By choosing the fac-[^{99m}Tc(CO)$_3$]$^+$ core as the radioactive label, we have taken into consideration the characteristic high kinetic inertness of Tc(I) tricarbonyl complexes. In particular, we expected to overcome the unstable radiolabeling that we have previously found when the **Au-DTDTPA** nanoplatform was labeled with ^{67}Ga. Ga^{3+} is a quite labile metal-ion and, in the absence of strong-donor multidentate chelators, readily undergoes transchelation processes involving biologically relevant molecules like transferrin, as we have observed in the case of ^{67}Ga-labelled **Au-DTDTPA**.[26,29] Previous reports describe the labelling of **Au-DTDTPA** nanoconstructs via the reduction of ^{99m}TcO$_4^-$ by SnCl$_2$.[33] However, this labeling approach involves medium oxidation states of Tc, like Tc(IV) or Tc(V), which have the tendency to form complexes with less kinetic inertness when compared with organometallic Tc(I) complexes. Technetium(I) tricarbonyl complexes usually display a high kinetic inertness and can be stabilized by a variety of bi- and tridentate chelators, including hard donors with amino or carboxylic acid coordination functions.[40–42] Hence, we anticipated that DTDTPA would provide a stable complexation of the fac-[^{99m}Tc(CO)$_3$]$^+$ core and should be a kinetically stable label for the follow-up of the in $vitro$/in $vivo$ fate of **Au-DTDTPA** nanoconstructs. Such kinetic inertness supports the notion that a multitude of bi- and tridentate chelators can stabilize the fac-[^{99m}Tc(CO)$_3$]$^+$ core, even in the presence of biologically relevant molecules, like aminoacids, peptides or proteins.[40] In particular, hard donor chelators ($e.g.$ iminodiacetic, lanthionine or DTPTA derivatives) displaying amino or carboxylic acid coordination functions form ^{99m}Tc(I) tricarbonyl complexes that are stable in $vivo$.[41,42]

The labeling of **BBN-Au-DTDTPA** with the fac-[^{99m}Tc(CO)$_3$]$^+$ core was done by reaction with the precursor [^{99m}Tc(H$_2$O)$_3$(CO)$_3$]$^+$ at pH ≈ 7, using a final nanoparticle concentration of 0.19 mg mL^{-1}. The reaction was conducted at 100 °C for 30 min, affording a maximum radiochemical yield of ≈75% (Scheme 2). The ^{99m}Tc-labeled AuNPs were purified by ultra-filtration to remove any unreacted tricarbonyl precursor, and recovered by redissolution in water. The purified **BBN-Au-DTDTPA-^{99m}Tc** were obtained with high radiochemical purity (>95%), as assessed by TLC with MeOH/6 M HCl (95 : 5) as the eluent (Fig. 4). Only purified nanoparticles were used in the stability and biological studies described below.

The in $vitro$ stability of **BBN-Au-DTDTPA-^{99m}Tc** was monitored in the presence of different biologically relevant solutions: NaCl 0.9% and PBS 0.1 M, at 37 °C. Additionally, challenge experiments were also performed for histidine and glutathione (GSH), which are both small biomolecules that are present in $vivo$. Histidine is a strong chelator towards the
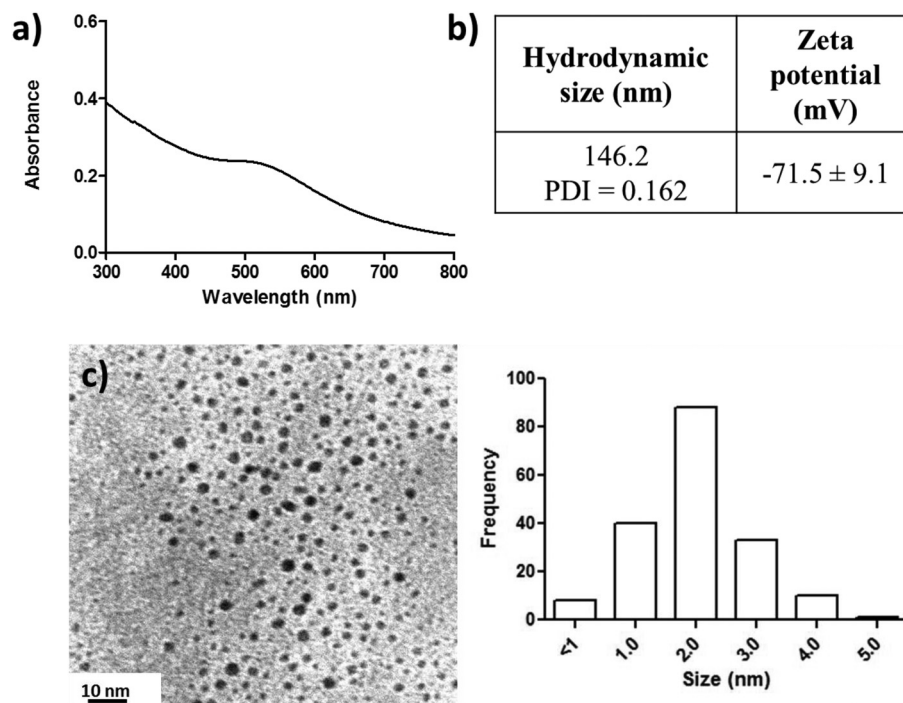
Fig. 3 (a) UV-Vis spectrum (8×10^{-2} mg mL^{-1}), (b) hydrodynamic size and zeta potential values (H$_2$O, pH $\approx$ 6), and (c) TEM image with respective size histogram for **BBN-Au-DTDTPA**.
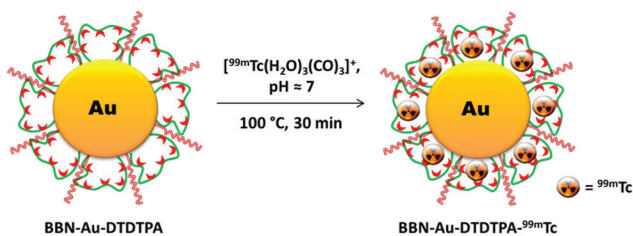
Scheme 2 Radiolabeling of **BBN-Au-DTDTPA** with ^{67}Ga.

fac-[^{99m}Tc(CO)$_3$]$^+$ unit, and is commonly used to check the kinetic inertness of Tc(I) tricarbonyl complexes in transchelation processes.[43] GSH also presents metal coordination properties and, in addition, as mentioned previously, it can also interfere with the Au–S and S–S bonds. Hence, we have considered that the GSH challenge experiments could give some indications on the possible detachment of the DTDTPA coating from the nanoparticles surface.

The *in vitro* stability of **BBN-Au-DTDTPA-^{99m}Tc** was studied by incubation in the presence of different biologically relevant media at 37 °C during different intervals of time (0–24 h) and by performing radio-TLC analysis at different time points. The radio-TLC analysis was done using ITLC-SG plates with MeOH/6 M HCl (95 : 5) as eluent. In this system, the radiolabeled AuNPs remain at R_f = 0, while ^{99m}Tc radiochemical species released from the nanoparticle surface are expected to migrate to the solvent front. The results obtained for the *in vitro* stability studies are presented in Fig. 5.

As shown in Fig. 5, **BBN-Au-DTDTPA-^{99m}Tc** showed high stability in the presence of 0.9% NaCl, 0.1 M PBS and 20 mM histidine. More than 90% of the AuNPs remain labeled with ^{99m}Tc, even after 24 h incubation at 37 °C. By contrast, GSH led to a very fast release of ^{99m}Tc; only $\approx$40% of the radioactivity is associated with the AuNPs for incubation times less than 1 h (Fig. 5). Taking into account the well-recognized affinity of histidine towards the [^{99m}Tc(CO)$_3$]$^+$ core, these results led us to consider that the GSH-mediated release of ^{99m}Tc from **BBN-Au-DTDTPA-^{99m}Tc** should not correspond to a simple transchelation process.

To understand this in detail, we have performed HPLC analysis of the supernatant of the reaction mixture obtained by incubation of **BBN-Au-DTDTPA-^{99m}Tc** with GSH, at 37 °C and for 4 h. Following incubation and prior to the HPLC analysis, it was confirmed that most of the radioactivity ($\approx$67%) was present in the analyzed supernatant. As shown in Fig. 6, the obtained HPLC chromatogram displays an unresolved set of peaks with the major ones having retention times (r.t.) centered at 26 min. None of these peaks correspond to fac-[^{99m}Tc(CO)$_3$(H$_2$O)$_3$]$^+$, which has a much shorter retention time (r.t. < 10 min) when analyzed under the same analytical conditions.

We have studied the labelling of GSH with the [^{99m}Tc(CO)$_3$]$^+$ core to check *trans*-chelation processes from the nanoconstruct coating to GSH. As can be seen in Fig. 6, the reaction of fac-[^{99m}Tc(CO)$_3$(H$_2$O)$_3$]$^+$ with GSH was not complete and led to a mixture of radioactive species. The HPLC chromatogram of the reaction mixture showed a major species with a
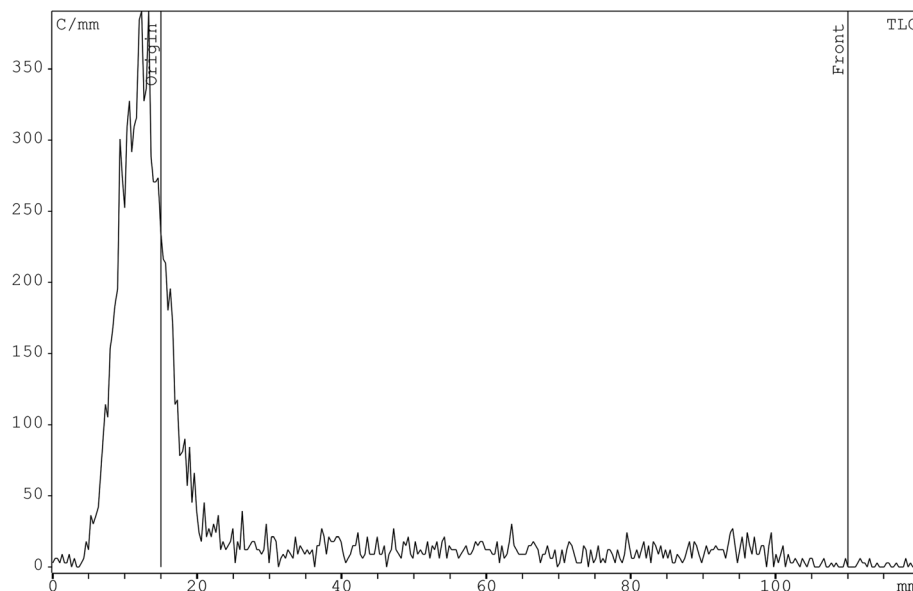
Fig. 4 Radiochromatogram of purified **BBN-Au-DTDTPA-^{99m}Tc**. Analysis was performed in ITLC-SG using 6 M HCl/MeOH (5 : 95) as eluent. In this system, **BBN-Au-DTDTPA-^{99m}Tc** remains at the application point ($R_f = 0$) and $[^{99m}Tc(H_2O)_3(CO)_3]^+$ shows $R_f = 1$.
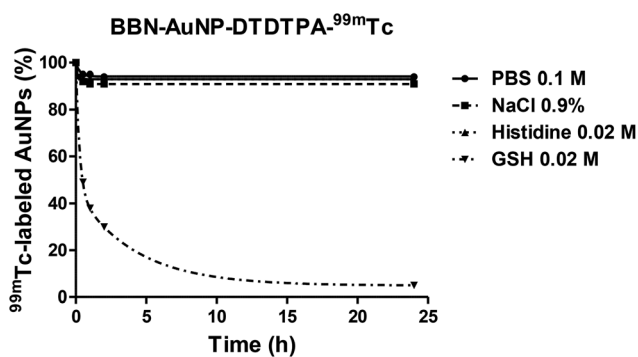
Fig. 5 *In vitro* stability of **BBN-Au-DTDTPA-^{99m}Tc** in different biologically relevant solutions.
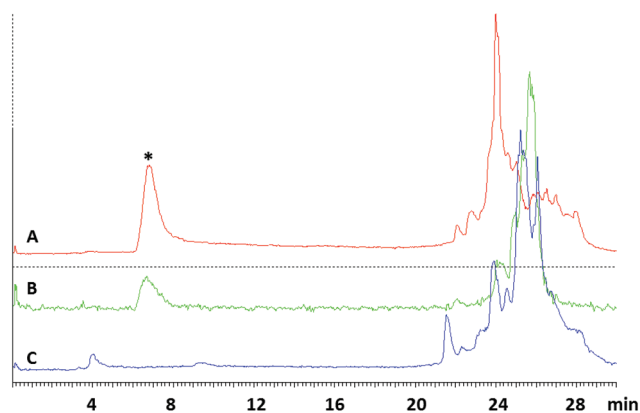
Fig. 6 HPLC chromatograms of: (A) reaction of *fac*-$[^{99m}Tc(CO)_3(H_2O)_3]^+$ with GSH (*ca.* 2 mM) at 100 °C for 30 min; (B) supernatant of the reaction of **BBN-Au-DTDTPA-^{99m}Tc** with GSH at 37 °C for 4 h, after separation of the nanoparticles by ultrafiltration; (C) reaction of DTDTPA (*ca.* 2 mM) with *fac*-$[^{99m}Tc(CO)_3(H_2O)_3]^+$ at 95 °C for 30 min; *$[^{99m}Tc(CO)_3(H_2O)_3]^+$.

retention time of *ca.* 24 min, which is eluted before the predominant radiochemical species that are formed in the reaction of **BBN-Au-DTDTPA-^{99m}Tc** with GSH. These data show that the GSH-mediated release of ^{99m}Tc from the AuNP surface does not involve predominantly a *trans*-chelation process, suggesting a more probably detachment of the ^{99m}Tc-labelled DTDTPA from the gold surface.

To validate the GSH mediated release of DTDTPA from AuNPs we have studied the $[^{99m}Tc(CO)_3]$-labeling of DTDTPA (with no nanoparticles), and performed the HPLC analysis of the complexes formed. The reaction of DTDTPA with *fac*-$[^{99m}Tc(CO)_3(H_2O)_3]^+$ was run at 95 °C for 30 min., using a 2 mM ligand concentration. Under these conditions, there was a complete consumption of the tricarbonyl precursor with formation of a mixture of ^{99m}Tc(I)-DTDTPA tricarbonyl complexes with retention times in the range 24–26 min, as shown by HPLC analysis of the reaction mixture (Fig. 6). DDTPA can act

as an ambivalent chelator towards the *fac*-$[^{99m}Tc(CO)_3]^+$ core, through the three carboxylic acid, three amine and even the two thiol groups, which can justify the formation of different complexes. The retention times of predominant ^{99m}Tc(I)-DTDTPA tricarbonyl complexes are almost coincident with those exhibited by the major ^{99m}Tc(I) species released from the reaction of **BBN-Au-DTDTPA-^{99m}Tc** with GSH (see radioHPLC traces (B) and (C) in Fig. 6).

Overall, these results indicate that in the presence of GSH there is no dissociation of $[^{99m}Tc(CO)_3]^+$ from the DTDTPA chelator, with subsequent *trans*-chelation to GSH. Most probably, GSH promotes the release of DTDTPA-^{99m}Tc(CO)$_3$ complexes

from the AuNPs by replacing the Au–S bonds involving DTDTPA or, alternatively, by cleaving the S–S bonds from the polymeric DTDTPA coating. Both possibilities are well documented in the literature and have been explored in several instances to design GSH-mediated drug delivery systems.[44] With our data, it is difficult to draw conclusions on preference. However, we can presume that the cleavage of the S–S bonds is more plausible, as these bonds at the outer surface of the nanoconstructs are more exposed to GSH action than the inner Au–S bonds are.

In vivo studies

Thereafter, we have investigated if the action of GSH that was observed *in vitro* will also be translated *in vivo*, by performing the following studies in normal CD1 mice: (i) biodistribution studies of **BBN-Au-DTDTPA-^{99m}Tc** in comparison with **DTDTPA-^{99m}Tc(CO)$_3$** and *fac*-[^{99m}Tc(CO)$_3$(H$_2$O)$_3$]$^+$, by gamma-counting measurements; (ii) radio HPLC analysis of the urine collected from mice injected with **BBN-Au-DTDTPA-^{99m}Tc** and **DTDTPA-^{99m}Tc(CO)$_3$**; (iii) quantification of the gold content in selected organs and tissues using NAA for comparison.

The mice were injected with **BBN-Au-DTDTPA-^{99m}Tc** and sacrificed at 1 h and 4 h p.i. Major organs were excised and their radioactivity measured as detailed in the Methods section. The results are presented in Fig. 7 and in ESI (Table S1†).

BBN-Au-DTDTPA-^{99m}Tc shows a fast blood clearance with a decrease of the circulating activity from 1.1 ± 0.1 to 0.4 ± 0.1 %ID g^{-1} at 1 h and 4 h p.i., respectively. There is also a rather fast rate of excretion being observed, with an overall excretion of 50% at 1 h p.i. The retained activity is mainly in the organs that are involved in excretory pathways, like the liver (4.2 ± 1.0 %ID g^{-1} at 4 h p.i.) and the kidney (31.3 ± 4.8 %ID g^{-1}, at 4 h p.i.). This biodistribution profile clearly contrasts with that exhibited by the *fac*-[^{99m}Tc(CO)$_3$(H$_2$O)$_3$]$^+$ precursor (see Fig. S2†), which has a very slow blood clearance (12.0 %ID g^{-1} at 1 h p.i) and a much lower rate of excretion (13.8 %ID) reflecting most probably its reactivity and ability to interact with blood proteins. These differences show that **BBN-Au-**

DTDTPA-^{99m}Tc does not release the *fac*-[^{99m}Tc(CO)$_3$]$^+$ *in vivo* by transchelation processes to proteins or other biological substrates.

BBN-Au-DTDTPA-^{99m}Tc has a fast overall excretion primarily *via* urine. Therefore, we have analyzed the urine of a CD-1 mice injected with these ^{99m}Tc-labeled nanoconstruct by radioTLC (Fig. S3†), in order to compare the chromatographic behavior of the excreted ^{99m}Tc-species with the injected **BBN-Au-DTDTPA-^{99m}Tc**. Most of the ^{99m}Tc (≈89%) migrated to $R_f ≈ 0.9$ indicating that the radiometal was released *in vivo* from the AuNP surface, as the injected **BBN-Au-DTDTPA-^{99m}Tc** present $R_f ≈ 0.0$ in the same chromatographic system (see Fig. 4).

The urine of the mice injected with **BBN-Au-DTDTPA-^{99m}Tc** and with **DTDTPA-^{99m}Tc(CO)$_3$** was analyzed by HPLC (Fig. 8, trace A). The obtained HPLC radiochromatograms are almost superimposable and show a profile very similar to that of the injected preparation of **DTDTPA-^{99m}Tc(CO)$_3$** (see Fig. 8, trace B). Altogether, these results indicate that [^{99m}Tc(CO)$_3$]$^+$ remains coordinated to DTDTPA and corroborate the *in vivo* release of the DTDTPA coating, most probably through GSH-mediated processes in agreement with the *in vitro* challenge experiments.

We have also evaluated the pharmacokinetics and biodistribution of **DTDTPA-^{99m}Tc(CO)$_3$** in the mice (see Table S2†). **DTDTPA-^{99m}Tc(CO)$_3$** has a blood clearance (1.0 ± 0.2 %ID g^{-1} at 4 h p.i.) and overall rate of excretion (46.2 ± 0.6 %ID at 4 h p.i.) slower than **BBN-Au-DTDTPA-^{99m}Tc** that presented 0.4 ± 0.1 %ID g^{-1} and 64.3 ± 0.9 %ID values for the same time point, respectively. One should not expect that both radioconjugates would present an identical biodistribution profile. First, a small part of ^{99m}Tc is excreted associated with the nanoparticles, *ca.* 10% according to the ITLC results (Fig. 8). Second, the GSH-mediated release of **DTDTPA-^{99m}Tc(CO)$_3$** must have its own kinetics and this can be expected to occur more easily at a intracellular level, where the concentration of GSH is highest.

Finally, we have compared the *in vivo* tracking of ^{99m}Tc and Au following intravenous administration of **BBN-Au-**
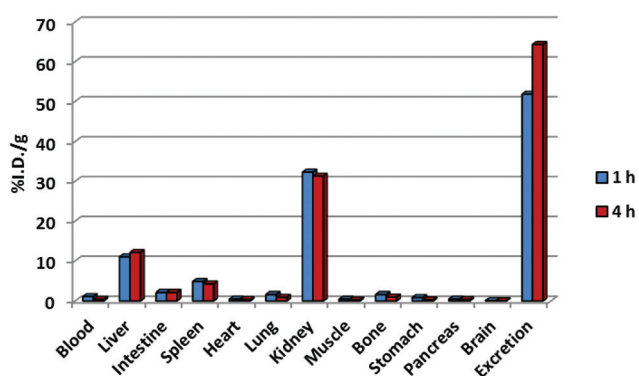
Fig. 7 Biodistribution results of **BBN-Au-DTDTPA-^{99m}Tc** in female CD-1 mice showing organ and tissue uptake (expressed in %ID g^{-1}) and overall excretion at 1 h and 4 h after i.v. administration.
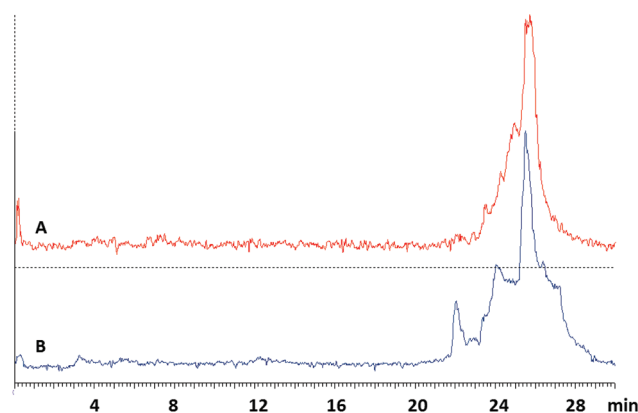
Fig. 8 HPLC radiochromatograms of urine samples collected at 1 h p.i. from CD-1 mice injected with: (A) **BBN-Au-DTDTPA-^{99m}Tc**; (B) **DTDTPA-^{99m}Tc(CO)$_3$**.

DTDTPA-^{99m}Tc by measuring the Au content of selected organs and tissues (blood, liver and urine) by NAA analysis (Fig. 9 and Table S3†).

The comparison of the NAA (Au content) and gamma-counting (^{99m}Tc content) biodistribution results showed that there are significant differences in the %ID g^{-1} of both metals, as follows: (i) the blood clearance observed for ^{99m}Tc is faster than that of Au (%ID g^{-1} (^{99m}Tc)/%ID g^{-1} (Au) = 0.37 at 4 h p.i.); (ii) the liver uptake is higher and more prolonged for ^{99m}Tc than for Au (%ID g^{-1} (^{99m}Tc)/%ID g^{-1} (Au) = 2.85 at 1 h p.i.); (iii) the pancreas uptake is higher for Au than for [99m]Tc (%ID g^{-1} (^{99m}Tc)/%ID g^{-1} (Au) = 0.39 at 4 h p.i.). These results show that Au and ^{99m}Tc have independent kinetics, which is consistent with the excretion of ^{99m}Tc in the form of **DTDTPA-[99m]Tc(CO)$_3$** released from the AuNPs.

An important point is the difference in ^{99m}Tc and Au uptake in the pancreas, an organ with high GRPr density;[45] for this reason, it is common to observe a high pancreatic uptake for BBN derivatives.[10,46] For instance, the group of Morales-Avila *et al.* described AuNPs targeted at GRPr with a pancreatic uptake as high as ≈39.83 %ID g^{-1} at 1 h p.i.[10] By contrast, **BBN-Au-DTDTPA-[99m]Tc** displayed a negligible ^{99m}Tc-uptake in the pancreas (maximum of 0.45 ± 0.03 %ID g^{-1} at 1 h p.i.) (see Fig. 7 and Table S1†). This can be related to the tendency of these AuNPs to release the [[99m]Tc(CO)$_3$]$^+$ coordinated to

DTDTPA monomers or oligomers, upon a probable GSH-mediated release of the DTDTPA covering. The highest Au content found in the pancreas might indicate the involvement of GRPr-mediated specific uptake for the **BBN-Au-DTDTPA** nanoparticles; however, this aspect was not investigated in the present work.

Conclusions

A thioacetic acid-containing BBN derivative was successfully conjugated to **Au-DTDTPA** nanoparticles to obtain **BBN-Au-DTDTPA**, which displayed high affinity towards GRPr. These nanoconjugates were efficiently labelled with the *fac*-[[99m]Tc(CO)$_3$]$^+$ core and the radioactive label resisted, *in vitro*, *trans*-chelation reactions with histidine, one of the most powerful tridentate chelators towards this Tc(ı) core. By contrast, GSH promoted a fast *in vitro* release of the radiolabel; a detailed *in vitro* and *in vivo* investigation proved that the release of the radiolabel is due to the detachment of the DTDTPA coating from the nanoparticle surface.

In an *in vivo* environment, GSH is very abundant and previous reports have demonstrated that GSH can lead to the release of thiolated molecules from AuNPs, either by replacement of Au–S bonds or cleavage of S–S bonds.[16–18,44,47] Both types of bonds are present in the **BBN-Au-DTDTPA** nanoconjugates and the results corroborate the effect of GSH on the nanoconjugates. However, with our data it would be hard to conclude which type of these bonds was directly involved in the DTDTPA release.

In summary, our research showed that **Au-DTDTPA** nano-platforms surface functionalized with a BBN analog retain binding affinity towards GRPr overexpressed in PC3 prostate cancer cells *in vitro*. This result proves the suitability of **Au-DTDTPA** for functionalization with biomolecules aiming to obtain target-specific nanoconstructs and suggests the judicial use of the nanoconstructs for selective release of therapeutic agents.

Acknowledgements

Fig. 9 (A) Uptake of Au in selected organs and tissues after **BBN-Au-DTDTPA-[99m]Tc** (*n* = 2) in CD1 mice, injected *via* the tail vein. Data are expressed as mean of percentages of injected dose per gram of tissue (%ID g^{-1}); (B) ratio (%ID g^{-1} of ^{99m}Tc)/(%ID g^{-1} of Au) for the selected organs/tissues.

References

1 J. Xie, S. Lee and X. Y. Chen, *Adv. Drug Delivery Rev.*, 2010, **62**, 1064–1079.

2 N. Ahmed, H. Fessi and A. Elaissari, *Drug Discovery Today*, 2012, **17**, 928–934.

3 E. K. Lim, T. Kim, S. Paik, S. Haam, Y. M. Huh and K. Lee, *Chem. Rev.*, 2015, **115**, 327–394.

4 Y. Xing, J. H. Zhao, P. S. Conti and K. Chen, *Theranostics*, 2014, **4**, 290–306.

5 R. Mout, D. F. Moyano, S. Rana and V. M. Rotello, *Chem. Soc. Rev.*, 2012, **41**, 2539–2544.

6 M. Arruebo, M. Valladares and A. Gonzalez-Fernandez, *J. Nanomater.*, 2009, 37.

7 L. D. Field, J. B. Delehanty, Y. C. Chen and I. L. Medintz, *Acc. Chem. Res.*, 2015, **48**, 1380–1390.

8 A. Rodzinski, R. Guduru, P. Liang, A. Hadjikhani, T. Stewart, E. Stimphil, C. Runowicz, R. Cote, N. Altman, R. Datar and S. Khizroev, *Sci. Rep.*, 2016, **6**.

9 S. Yook, Y. J. Lu, J. J. Jeong, Z. L. Cai, L. Tong, R. Alwarda, J. P. Pignol, M. A. Winnik and R. M. Reilly, *Biomacromolecules*, 2016, **17**, 1292–1302.

10 A. N. Mendoza-Sanchez, G. Ferro-Flores, B. E. Ocampo-Garcia, E. Morales-Avila, F. D. Ramirez, L. M. De Leon-Rodriguez, C. L. Santos-Cuevas, L. A. Medina, E. L. Rojas-Calderon and M. A. Camacho-Lopez, *J. Biomed. Nanotechnol.*, 2010, **6**, 375–384.

11 B. L. Allen, J. D. Johnson and J. P. Walker, *ACS Nano*, 2011, **5**, 5263–5272.

12 M. M. Dcona, Q. Yu, J. A. Capobianco and M. C. T. Hartman, *Chem. Commun.*, 2015, **51**, 8477–8479.

13 X. Guo, C. L. Shi, J. Wang, S. B. Di and S. B. Zhou, *Biomaterials*, 2013, **34**, 4544–4554.

14 B. Khorsand, G. Lapointe, C. Brett and J. K. Oh, *Biomacromolecules*, 2013, **14**, 2103–2111.

15 H. Y. Wen, H. Q. Dong, W. J. Xie, Y. Y. Li, K. Wang, G. M. Pauletti and D. L. Shi, *Chem. Commun.*, 2011, **47**, 3550–3552.

16 M. McCully, Y. Hernandez, J. Conde, P. V. Baptista, J. M. de la Fuente, A. Hursthouse, D. Stirling and C. C. Berry, *Nano Res.*, 2015, **8**, 3281–3292.

17 Y. Ding, Z. W. Jiang, K. Saha, C. S. Kim, S. T. Kim, R. F. Landis and V. M. Rotello, *Mol. Ther.*, 2014, **22**, 1075–1083.

18 Q. Y. Bao, D. D. Geng, J. W. Xue, G. Zhou, S. Y. Gu, Y. Ding and C. Zhang, *Int. J. Pharm.*, 2013, **446**, 112–118.

19 J. D. G. Correia, A. Paulo, P. D. Raposinho and I. Santos, *Dalton Trans.*, 2011, **40**, 6144–6167.

20 A. B. de Barros, A. Tsourkas, B. Saboury, V. N. Cardoso and A. Alavi, *EJNMMI Res.*, 2012, **2**, 39.

21 W. G. Kreyling, A. M. Abdelmonem, Z. Ali, F. Alves, M. Geiser, N. Haberl, R. Hartmann, S. Hirn, D. J. de Aberasturi, K. Kantner, G. Khadem-Saba, J. M. Montenegro, J. Rejman, T. Rojo, I. R. de Larramendi, R. Ufartes, A. Wenk and W. J. Parak, *Nat. Nanotechnol.*, 2015, **10**, 619–+.

22 J. Gao, X. Y. Huang, H. Liu, F. Zan and J. C. Ren, *Langmuir*, 2012, **28**, 4464–4471.

23 E. C. Dreaden, B. E. Gryder, L. A. Austin, B. A. T. Defo, S. C. Hayden, M. Pi, L. D. Quarles, A. K. Oyelere and M. A. El-Sayed, *Bioconjugate Chem.*, 2012, **23**, 1507–1512.

24 B. Jang, S. Park, S. H. Kang, J. K. Kim, S.-K. Kim, I.-H. Kim and Y. Choi, *Quant. Imaging Med. Surg.*, 2012, **2**, 1–11.

25 Y. H. Kim, J. Jeon, S. H. Hong, W. K. Rhim, Y. S. Lee, H. Youn, J. K. Chung, M. C. Lee, D. S. Lee, K. W. Kang and J. M. Nam, *Small*, 2011, **7**, 2052–2060.

26 F. Silva, A. Zambre, M. P. C. Campello, L. Gano, I. Santos, A. M. Ferraria, M. J. Ferreira, A. Singh, A. Upendran, A. Paulo and R. Kannan, *Bioconjugate Chem.*, 2016, **27**, 1153–1164.

27 N. Chanda, R. Shukla, K. V. Katti and R. Kannan, *Nano Lett.*, 2009, **9**, 1798–1805.

28 N. Chanda, V. Kattumuri, R. Shukla, A. Zambre, K. Katti, A. Upendran, R. R. Kulkarni, P. Kan, G. M. Fent, S. W. Casteel, C. J. Smith, E. Boote, J. D. Robertson, C. Cutler, J. R. Lever, K. V. Katti and R. Kannan, *Proc. Natl. Acad. Sci. U. S. A.*, 2010, **107**, 8760–8765.

29 D. C. P. Chen, B. Newman, R. M. Turkall and M. F. Tsan, *Eur. J. Nucl. Med.*, 1982, **7**, 536–540.

30 P. J. Debouttiere, S. Roux, F. Vocanson, C. Billotey, O. Beuf, A. Favre-Reguillon, Y. Lin, S. Pellet-Rostaing, R. Lamartine, P. Perriat and O. Tillement, *Adv. Funct. Mater.*, 2006, **16**, 2330–2339.

31 I. Miladi, C. Alric, S. Dufort, P. Mowat, A. Dutour, C. Mandon, G. Laurent, E. Brauer-Krisch, N. Herath, J. L. Coll, M. Dutreix, F. Lux, R. Bazzi, C. Billotey, M. Janier, P. Perriat, G. Le Duc, S. Roux and O. Tillement, *Small*, 2014, **10**, 1116–1124.

32 C. Alric, J. Taleb, G. Le Duc, C. Mandon, C. Billotey, A. Le Meur-Herland, T. Brochard, F. Vocanson, M. Janier, P. Perriat, S. Roux and O. Tillement, *J. Am. Chem. Soc.*, 2008, **130**, 5908–5915.

33 C. Alric, I. Miladi, D. Kryza, J. Taleb, F. Lux, R. Bazzi, C. Billotey, M. Janier, P. Perriat, S. Roux and O. Tillement, *Nanoscale*, 2013, **5**, 5930–5939.

34 A. Zambre, F. Silva, A. Upendran, Z. Afrasiabi, Y. Xin, A. Paulo and R. Kannan, *Chem. Commun.*, 2014, **50**, 3281–3284.

35 R. Alberto, K. Ortner, N. Wheatley, R. Schibli and A. P. Schubiger, *J. Am. Chem. Soc.*, 2001, **123**, 3135–3136.

36 A. C. Fernandes, J. P. Santos, J. G. Marques, A. Kling, A. R. Ramos and N. P. Barradas, *Ann. Nucl. Energy*, 2010, **37**, 1139–1145.

37 M. A. Gouveia, M. I. Prudencio, I. Morgado and J. M. P. Cabral, *J. Radioanal. Nucl. Chem.*, 1992, **158**, 115–120.

38 M. A. Gouveia and M. I. Prudencio, *J. Radioanal. Nucl. Chem.*, 2000, **245**, 105–108.

39 *NIST X-ray Photoelectron Spectroscopy Database, Version 4.1*, National Institute of Standards and Technology, Gaithersburg, 2012; http://srdata.nist.gov/xps/ (visited 14, April, 2014).

40 G. R. Morais, A. Paulo and I. Santos, *Organometallics*, 2012, **31**, 5693–5714.

41 M. Lipowska, H. Y. He, E. Malveaux, X. L. Xu, L. G. Marzilli and A. Taylor, *J. Nucl. Med.*, 2006, **47**, 1032–1040.

42 D. Rattat, C. Terwinghe and A. Verbruggen, *Tetrahedron*, 2005, **61**, 9563–9568.

43 R. Schibli, R. La Bella, R. Alberto, E. Garcia-Garayoa, K. Ortner, U. Abram and P. A. Schubiger, *Bioconjugate Chem.*, 2000, **11**, 345–351.

44 G. Han, R. Hong, J. Fernandez, B. J. Kim, N. S. Forbes and V. M. Rotello, *Abstr. Pap. Am. Chem. Soc.*, 2006, **231**.

45 J. Schuhmacher, H. Zhang, J. Doll, H. R. Macke, R. Matys, H. Hauser, M. Henze, U. Haberkorn and M. Eisenhut, *J. Nucl. Med.*, 2005, **46**, 691.

46 X. Montet, R. Weissleder and L. Josephson, *Bioconjugate Chem.*, 2006, **17**, 905–911.

47 X. Y. Wang, X. P. Cai, J. J. Hu, N. M. Shao, F. Wang, Q. Zhang, J. R. Xiao and Y. Y. Cheng, *J. Am. Chem. Soc.*, 2013, **135**, 9805–9810.